An enthalpy landscape view of homogeneous melting in crystals

Alex M. Nieves and Talid Sinno[a)]
Department of Chemical and Biomolecular Engineering, University of Pennsylvania, Philadelphia, Pennsylvania 19104, USA

(Received 18 March 2011; accepted 14 July 2011; published online 17 August 2011)

A detailed analysis of homogeneous melting in crystalline materials modeled by empirical interatomic potentials is presented using the theory of inherent structures. We show that the homogeneous melting of a perfect, infinite crystalline material can be inferred directly from the growth exponent of the inherent structure density-of-states distribution expressed as a function of formation enthalpy. Interestingly, this growth is already established by the presence of very few homogeneously nucleated point defects in the form of Frenkel pairs. This finding supports the notion that homogeneous melting is appropriately defined in terms of a one-phase theory and does not require detailed consideration of the liquid phase. We then apply this framework to the study of applied hydrostatic compression on homogeneous melting and show that the inherent structure analysis used here is able to capture the correct pressure-dependence for two crystalline materials, namely silicon and aluminum. The coupling between the melting temperature and applied pressure arises through the distribution of formation volumes for the various inherent structures. © *2011 American Institute of Physics*. [doi:10.1063/1.3624656]

I. INTRODUCTION

Melting has been the focus of studies for centuries, and remains a highly debated and researched topic. Thermodynamically, melting is described as a first order phase transition in which a solid phase of a material transforms into a liquid phase. Within this framework, melting takes place at a temperature T_M in which the solid free energy of the solid and liquid are equal. Due to the discontinuous nature of first order transitions, the latent heat of melting, ΔH_M, is required for the transition, which is also generally accompanied by a change in volume, ΔV_M, due to a difference in the density of the two phases at T_M.

In order for a material to melt precisely at T_M, a heterogeneous nucleation source for the liquid phase must be present. Most commonly, solid materials contain surfaces,[1,2] grain boundaries,[3] and other types of microstructure that melt locally at temperatures lower than or at T_M. In some special cases, however, the creation of a liquid nucleation source can be suppressed and the material can be superheated to temperatures above T_M while remaining in a metastable solid phase. Examples of such cases include coated nano-particles[4,5] and laser irradiation of bulk solids.[6,7] Here, the phase transition must be initiated homogeneously from within the bulk of the material; it is this process that is the focus of the present study.

There is still no consensus within the literature regarding a precise definition of homogeneous melting, and numerous theories have been put forward. One class of theories is based on the existence of "catastrophies," in which some thermodynamic or mechanical quantity in the solid becomes equal to its counterpart in the liquid phase at some temperature above the thermodynamic melting point. Example measures include internal energy,[8] entropy,[9,10] volume,[11] and elasticity.[11] Another class of theories arises from considering the mechanical behavior of the crystalline solid as temperature increases. One particularly well-known example is the Lindemann criterion, which posits that lattice instability leads to melting at a temperature in which the magnitude of atomic vibrations surpasses a critical value.[12,13] Another is the Born criterion, which suggests that a material will melt when one of the shear moduli of the system vanishes.[14] A third class of theories focuses on the role of defect nucleation (e.g., Frenkel, or interstitial-vacancy, pairs) as an important component in homogenous melting. In particular, the formation of clusters of such defects has been interpreted either to lead to critically sized liquid regions that act as nucleation sites for further melting,[15–19] or to a lattice instability through percolation of defects throughout the bulk material.[9–11]

Connections between homogeneous mechanical models (i.e., the Lindemann or Born theories) and the notion of defect-mediated melting have been established in the literature. For example, using molecular dynamics of a Lennard-Jones system, Jin *et al.*[17] were able to connect the Lindemann and Born melting mechanisms by focusing only on clusters of defective atoms, rather than the entire system. More recently, the conceptual framework of the inherent structure landscape (ISL) (Refs. 20 and 21) has been applied in the context of homogeneous melting. Within the ISL framework, the total partition function of a system is approximated by a sum over all the energy (or enthalpy) basins within the potential energy (or enthalpy) landscape; each of these basins corresponds to a distinct, mechanically stable configuration of the system.[22–29] Recently, Chakravarty *et al.*[30] employed ISL theory to generalize the Lindemann picture by computing atomic return distance distributions to local minima from multiple

a)Author to whom correspondence should be addressed. Electronic mail: talid@seas.upenn.edu.

instantaneous configurations in a Lennard-Jones system as a function of temperature and pressure for both solid and liquid phases. It was found that return distances to various inherent structures exhibit sudden changes in the vicinity of the melting transition and therefore can be used to signal phase transitions with significantly more information than that provided by the conventional Lindemann parameter.

The interpretation of homogeneous melting of crystals in the context of ISL theory was pioneered by Stillinger and Weber[31] using a somewhat different conceptual approach. Here, molecular dynamics simulations were employed to identify multiple inherent structures corresponding to spontaneously formed IV pairs in an empirical model of a bcc crystal. Using a simplified analytical partition function model, it was demonstrated that the expected number of IV pairs became singular at a temperature close to the established melting temperature, thereby signaling the transition. The model also incorporated the notion of "defect softening" in which each additional IV pair caused the crystal to become softer, corresponding to higher vibrational entropy; interestingly, without this element it was not possible to predict a divergent behavior in the defect density at a finite temperature as required for signaling a first order transition.

In essence, the results of Stillinger and Weber[31] suggest that homogeneous melting is related directly to the ISL structure (i.e., basin shapes and distribution of inherent structures), which is not connected in an obvious fashion to the Lindemann and Born mechanical frameworks. Related conclusions were presented in Ref. 32 for order-disorder transitions in binary alloys. Here, it was shown that an exponential growth in the density of inherent structures as a function of energy corresponds to a divergence in the specific heat at a critical temperature that is quantitatively related to the growth exponent of the IS density distribution. Finally, ISL theory has been similarly applied to protein folding,[33,34] where once again it has been shown that the growth rate of the density of inherent structures with energy is closely linked to the folding temperature. The latter is an analogue of the melting temperature in crystalline atomic systems and exhibits much of the same thermodynamic characteristics.

In this paper, we apply ISL theory in the spirit of the latter studies, focusing on the link between the structure of an ISL and homogeneous melting in two distinct prototypical crystalline materials, silicon and aluminum. We first compare and contrast the quantitative connections between the ISL and melting in these two materials. Then, we demonstrate that IS theory, properly applied, is able to capture subtle effects such as coupling between applied stress and the homogeneous melting temperature. The remainder of the paper is structured as follows. In Sec. II, we briefly present the specific IS framework employed here. In Sec. III, the simulation methodology employed throughout this work is presented. An enthalpy landscape analysis of melting at zero pressure is discussed in Sec. IV. The effect of pressure on homogeneous melting is addressed in Sec. V. Finally, conclusions are presented in Sec. VI.

II. INHERENT STRUCTURES AND DENSITY-OF-STATES ANALYSIS

In this section, we briefly summarize the particular ISL framework that is used to analyze the following simulation results. We consider first the constant number of particles-volume-temperature (NVT) ensemble, and then address the more experimentally relevant constant-pressure (NPT) situation. The Helmholtz free energy is related to the (classical) canonical partition function by the relation

$$\beta F = -\ln Z(N, \beta, V), \tag{1}$$

where $\beta = 1/kT$, V is the system volume and

$$Z = \frac{1}{N}\frac{1}{\Lambda^{3N}}\int \exp(-\beta E(\mathbf{r}^N))d\mathbf{r}^N. \tag{2}$$

In Eq. (2), $\Lambda = (\beta h^2/2\pi m)^{1/2}$ is the thermal de Broglie wavelength, and $E(\mathbf{r}^N)$ is the potential energy of the system that depends on the 3N-dimensional position vector, $\mathbf{r}^N$. Using the ISL description of the energy landscape, Eq. (2) can be rewritten as[20]

$$Z = \frac{1}{\Lambda^{3N}}\int g(E_\alpha)\exp(-\beta E_\alpha)\exp(-\beta F_{vib}(\beta, E_\alpha))\,dE_\alpha, \tag{3}$$

where E_α is the potential energy of inherent structure α, and $g(E_\alpha)$ is the density-of-states (DOS) for the distribution of basins within the landscape. The quantity $F_{vib}(\beta, E_\alpha)$ represents the vibrational free energy of the basin with minimum energy, E_α.

Next, we define a single combined density-of-states distribution that includes both vibrational and configurational states, i.e.,

$$G'(\beta, E_\alpha) \equiv g(E_\alpha)\exp(-\beta F_{vib}(\beta, E_\alpha)). \tag{4}$$

For the perfect crystal configuration, $g(E^P) = 1$, and $G'(\beta, E^P) = \exp(-\beta F_{vib}(\beta, E^P))$, where E^P is the perfect crystal energy. Now, a density-of-states function can be defined in terms of formation energies,

$$G(\beta, \Delta E_\alpha) \equiv \frac{G'(\beta, E_\alpha)}{G'(\beta, E^P)} = g(E_\alpha)\exp(-\beta \Delta F_{vib}(E_\alpha)), \tag{5}$$

where $\Delta E_\alpha \equiv E_\alpha - E^P$ and $\Delta F_{vib}(E_\alpha) \equiv F_{vib}(\beta, E_\alpha) - F_{vib}(\beta, E^P)$ are the formation energy and vibrational free energy of basin α. The vibrational free energy of formation can be further simplified by invoking the harmonic approximation,[35] i.e.,

$$F_{vib}(\beta, E_\alpha) = kT\ln\left(\prod_q^{3(N-1)}(\beta h \upsilon_q(E_\alpha))\right), \tag{6}$$

where $\upsilon_q(E_\alpha)$ are the normal modes of basin α. Noting that $g(E_\alpha) = g(\Delta E_\alpha)$, and substituting into Eq. (5) provides a temperature-invariant density-of-states in terms of formation properties,

$$G(\Delta E_\alpha) = g(\Delta E_\alpha)\left[\prod_m^{3(N-1)}(\upsilon_m(E_\alpha))\Big/\prod_n^{3(N-1)}(\upsilon_n^P)\right]. \tag{7}$$

Using this density-of-states definition, Eq. (3) can be written entirely in terms of formation energy as

$$Z = \frac{\Omega^P(\beta)}{\Lambda^{3N}} \int G(\Delta E_\alpha) \exp(-\beta \Delta E_\alpha)\, d\Delta E_\alpha, \tag{8}$$

where $\Omega^P(\beta) = G'(\beta, E^P)\exp(-\beta E^P)$ is a temperature-dependent constant defined only on the reference configuration.

The above formalism readily can be extended to the isobaric-isothermal (NPT) ensemble which is characterized by an *enthalpy* landscape.[29,36] The key result is that the isothermal-isobaric partition function can be written in an analogous form to Eq. (3) i.e.,

$$Y(N, P, T) \propto \int g(H_\alpha) \exp(-\beta H_\alpha) \times \exp(-\beta \tilde{F}_{vib}(\beta, H_\alpha)) dH_\alpha, \tag{9}$$

where P is the pressure, H_α is the enthalpy of the inherent structure, $\tilde{F}_{vib}(\beta, H_\alpha)$ is the vibrational free energy of basin α within the NPT ensemble. Similar considerations used to derive Eq. (8) can be applied to give

$$Y \sim \int G(\Delta H_\alpha) \exp(-\beta \Delta H_\alpha)\, d\Delta H_\alpha. \tag{10}$$

In Eq. (10), the formation enthalpy is calculated as $\Delta H_\alpha = \Delta E_\alpha + P\Delta V_\alpha$, where $\Delta V_\alpha \equiv V_\alpha - V^P$ is the formation volume of a particular configuration that corresponds to basin α relative to the volume of the perfect crystal, V^P.

III. CALCULATION OF THE DENSITY-OF-STATES DISTRIBUTION

Throughout this work, molecular dynamics (MD) simulations are employed to generate the density-of-states distribution. The distribution is formed by taking periodic snapshots of atomic coordinates and quenching them using conjugate-gradient energy minimizations. MD simulation details are provided in Sec. III A. The result from each quench gives the local IS formation energy, ΔE_α, of the current basin. A histogram of visited formation energies is kept and used to calculate a probability distribution. For the results presented in the following sections, the visitation histogram is collected into energy/enthalpy bins of width 0.1 eV. For an NVT simulation at temperature, T_{sim}, this probability distribution is given by[23,25,33]

$$P(\Delta E_\alpha, \beta_{sim}) = C G(\Delta E_\alpha) \exp(-\beta_{sim} \Delta E_\alpha), \tag{11}$$

where C is a constant. The DOS distribution therefore can be extracted from the probability distribution by rearranging Eq. (11) so that

$$G(\Delta E_\alpha) \sim P(\Delta E_\alpha, \beta_{sim}) \exp(\beta_{sim} \Delta E_\alpha). \tag{12}$$

Note that $G(\Delta E_\alpha)$ is known only up to the constant C--if needed, this constant can be determined by anchoring the density-of-states to a known value at a given formation energy.[25] However, as will be shown later, the knowledge of C is not required for the analysis of melting. Similar considerations apply to the constant pressure situation.

A. Simulation details

Two empirical interaction potentials are used throughout the following simulations: the silicon Environment-Dependent Interatomic Potential (EDIP) potential[37] and an embedded-atom method (EAM) potential for aluminum.[38] Our choice of these two material systems is motivated by the fact that while Al exhibits the usual expansion upon melting ($\Delta V_M > 0$), liquid Si is denser than crystalline Si, i.e., $\Delta V_M < 0$. In broad terms, the different behaviors are related to the fact that the fcc lattice is more densely packed than the diamond one; in Sec. V, we discuss in detail how melting in these two material systems differs under the influence of applied pressure.

Although many potential models exist for both materials, these particular potentials were selected mainly on the basis that they are of very different functional forms to demonstrate the generality of the observations in the following sections. Additionally, for silicon, the Stillinger-Weber potential (SW) (Ref. 39) is also employed at various points to further demonstrate that the specific form of the potential does not alter our conclusions. While the EDIP potential has been shown to provide a very good representation of point defects and defect cluster thermodynamics,[25,26,40,41] the SW potential does offer a better description of the liquid state.[42] The thermodynamic melting temperature for EDIP silicon is about 1520 K,[25,42] for SW silicon about 1685 K,[39] while for aluminum modeled by the specific EAM variant used here it is 929 K.[38]

All MD simulations and associated energy minimizations were performed using the LAMMPS software package.[43] All calculations were based on cubic simulation cells containing initially perfectly crystalline configurations (diamond for Si and fcc for Al) subjected to periodic boundary conditions. Simulation cell sizes ranged from 2744 to 238 328 atoms. Unless otherwise stated, simulations were performed in the NPT ensemble using the Nosé-Hoover thermostat and barostat and the time step was fixed at 1 fs. For each run, the system first was equilibrated for 3×10^5 time steps, after which snapshots of the atomic coordinates were taken every 200 time steps and quenched to the IS structure of the current basin using constant-pressure energy minimizations. For all cases, multiple seeds were used to generate the total number of sampled local minima, which ranged from about 80 000 to 200 000, corresponding to 16–40 million MD time steps. The number of sampled basins used for each case was determined by monitoring the convergence of the PDF with respect to additional data. The convergence criterion for the minimizations was chosen based on the 2-norm of the force vector, i.e., $\|F\|_2 < 10^{-2}$, where

$$\|F\|_2 = \left\{ \sum_i \left[\left(f_i^x\right)^2 + \left(f_i^y\right)^2 + \left(f_i^z\right)^2 \right] \right\}^2, \tag{13}$$

and f_i^a is the force component of atom i on the direction of a. For each minimization during the sampling process, the potential energy and volume for each IS were recorded and used to find the formation energy and formation volume of the current configuration.

IV. HOMOGENEOUS MELTING AT ZERO PRESSURE

As mentioned in the Introduction, several prior literature studies have already linked the behavior of density-of-states (DOS) distributions of inherent structures to phase transitions. In particular, a DOS function that exhibits exponential growth with respect to energy is thought to signal a phase transition such as melting.[25,32,33] In this section, we consider the qualitative features of formation enthalpy probability distribution functions (PDFs) and the corresponding DOS functions for both EDIP-Si and EAM-Al in the context of homogeneous melting of perfect crystals at zero pressure. Some results for the SW-Si also are shown for comparison. For the EDIP-Si case, we use a 4096-atom simulation cell at 1900 K, for the SW-Si, 4096 atoms at 2225 K, and for EAM-Al, 4000 atoms at 1090 K. All three MD-NPT simulation temperatures correspond to significant superheating to allow for sampling of a wide range of inherent structures without resulting in homogeneous melting. Note that the actual amount of superheating in each simulation influences the range of enthalpies sampled but does not affect estimates of the underlying density-of-states distributions.

The resulting formation enthalpy PDFs for Si and Al are shown in Figures 1–3 for the three potentials; all PDFs are normalized to unit area. There are several features that are common to all three cases. First, the distribution of formation enthalpies sampled spans about 25–30 eV. At lower enthalpies a series of regularly spaced, distinct peak collections are observed, whereas at higher formation enthalpies the separation between these peak collections becomes less distinct; this feature is less noticeable in the EAM case but is still apparent by the decreasing peak-to-trough height between each peak collection as the formation enthalpy increases. The dashed straight line on each figure is a guide to the eye to show the apparently exponentially decaying envelope defined by the dominant peak in each collection across most of the enthalpy range. The implications of this envelope with regards to homogeneous melting are discussed in more detail later in the paper.

In all three cases, the distinct peak collections represent configurations associated with a fixed integral number of interstitial-vacancy (IV) pairs as denoted by the annotation at the top of each figure; we refer to each collection of peaks as a *macrostate*, defined solely by the number of IV pairs. The different individual peaks (*microstates*) in each macrostate, represent the various configurations associated with a given number of IV pairs; representative configurations are shown in the insets for Figures 1–3. Here, atoms are labeled (by the large red spheres) if their enthalpy differs by more than 1% of that of a perfect lattice atom (for Si) or if their centrosymmetry parameter[44] is larger than 1 (for Al). For example, a single IV pair can assume several different microstates, including a fully dissociated state where the self-interstitial and vacancy are separated by several atoms. In fact, while both Si potentials predict that the most favorable IV pair microstate is a combined defect (i.e., a Frenkel pair), the EAM potential predicts a dissociated IV pair (i.e., the vacancy and self-interstitial are separated by multiple lattice sites) as the most favorable microstate (see insets of Figures 1–3). Thus,

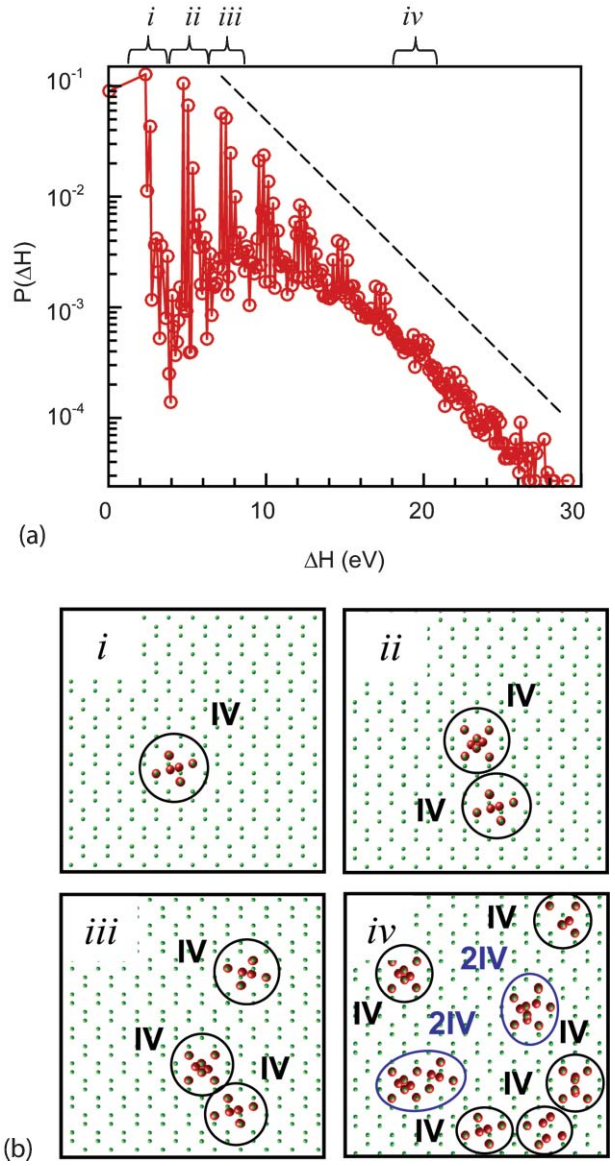

FIG. 1. (a) Zero-pressure probability distribution functions of inherent structure formation enthalpies for EDIP-Si at 1900 K. Dashed line is a guide to highlight exponential decay envelope. (b) Sample configurations for EDIP-Si inherent structures; (i) 2.38 eV, (ii) 4.76 eV, (iii) 7.17 eV, and (iv) 21.75 eV. Various defect structures are circled--self-interstitial (I), vacancy (V), Frenkel pair (IV), and clusters of each (2I, 2V, and 2IV).

for multiple IV pairs in Al, the dissociation tends to favor the formation of spatially separated interstitial and vacancy clusters, while for Si, IV pairs tend to cluster intact—however, both types of clusters can be observed in both systems. This is one example of a mechanistic difference in the defect-mediated homogeneous melting between the two material models, even though both are generally driven by Frenkel pair nucleation.

The increasing number of microstates within each macrostate as the formation enthalpy increases smears the probability distribution function, which becomes almost continuous at higher enthalpies. Although the EAM potential predicts a sparser inherent structure landscape for Al (at least for the enthalpy range shown here), this effect still is clearly operational in the Al case as the probability in each peak collection

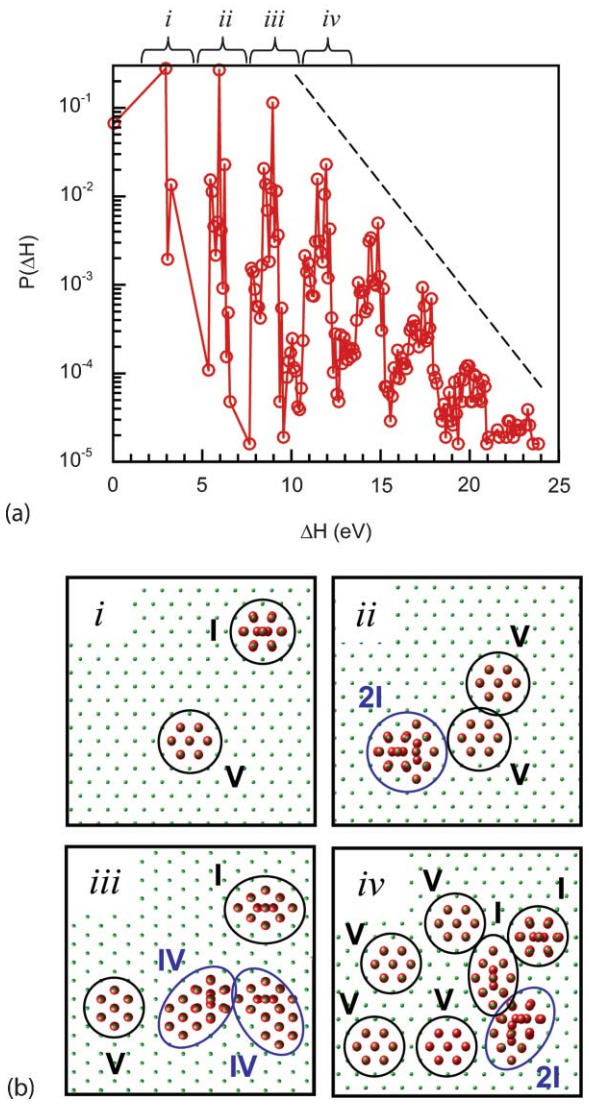

FIG. 2. (a) Zero-pressure probability distribution functions of inherent structure formation enthalpies for EAM-Al at 1090 K. Dashed line is a guide to highlight exponential decay envelope. (b) Sample configurations for EAM-Al inherent structures; (i) 2.98 eV, (ii) 5.53 eV, (iii) 8.92 eV, and (iv) 11.43 eV. See Figure 1 caption for assignments.

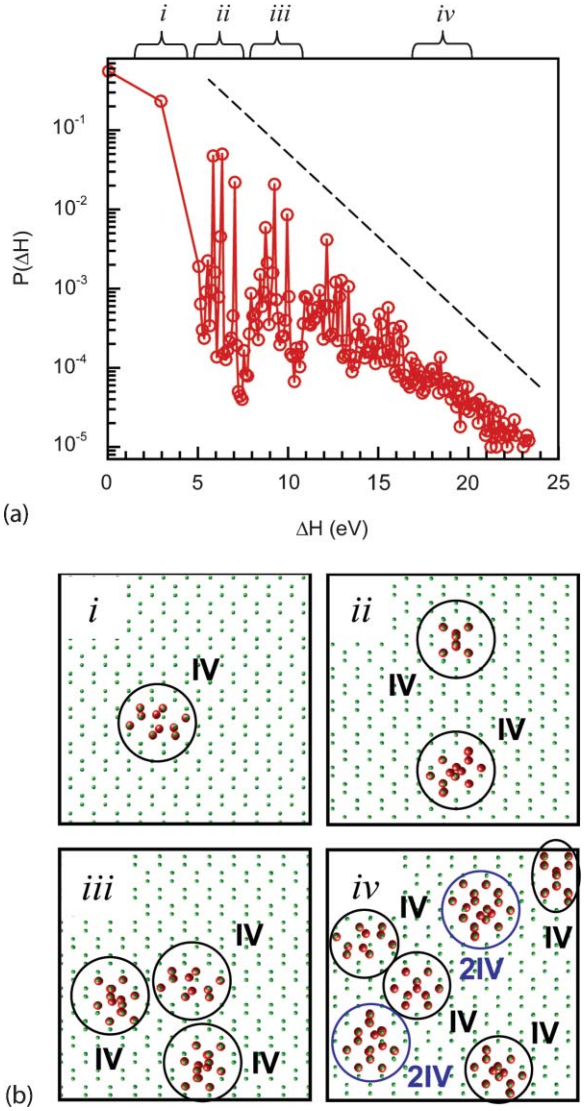

FIG. 3. (a) Zero-pressure probability distribution functions of inherent structure formation enthalpies for SW-Si at 2225 K. Dashed line is a guide to highlight exponential decay envelope. (b) Sample configurations for SW-Si inherent structures; (i) 2.93 eV, (ii) 5.85 eV, (iii) 8.80 eV, and (iv) 21.86 eV. See Figure 1 caption for assignments.

becomes more evenly distributed across several different inherent structures. The large number of configurational states introduced by the homogeneously nucleated defects arises from the fact that numerous local minima in the enthalpy (and energy) landscape exist over relatively small off-lattice atomic rearrangements.[25] The resulting configurational entropy can significantly alter the thermodynamic, structural, and transport properties of defects in crystalline materials at elevated temperature.[40,45,46]

The DOS functions corresponding to the PDFs shown in Figures 1–3 can be obtained by using Eq. (12), as shown in Figure 4 for all three potentials. All DOS functions presented here are plotted so that the density-of-states (which includes both configurational and vibrational contributions) is assigned a value of unity for the perfect crystal configuration, i.e., the DOS distributions are specified only up to an unknown constant. Although it is straightforward to compute the vibrational free energy of the perfect crystal using, for example, the quasi-harmonic approximation,[35,47] only the slope of the DOS is of relevance for the ensuing analysis.

The DOS distributions are all found to be exponentially increasing with formation enthalpy. Moreover, the exponent governing the distributions appears to be approximately constant across the entire enthalpy range considered here. Exponential fits are represented by the thick black lines in Figure 4 so that

$$G_{eff}(\Delta H) = \alpha_{eff} \exp(\beta_{eff} \Delta H), \tag{14}$$

where α_{eff} is equal to unity for a defect-free system and $\beta_{eff} \equiv 1/kT_{eff}$ is the slope of the curve, which defines an effective critical temperature that corresponds to the exponential growth in the DOS.[32,33] Note that both configurational and vibrational "states" are included in the DOS distributions and therefore contribute to the extracted critical temperature. The critical temperature for EDIP-Si is found to be ~2000 K, for SW-Si about 2385 K, while for Al it is about 1120 K.

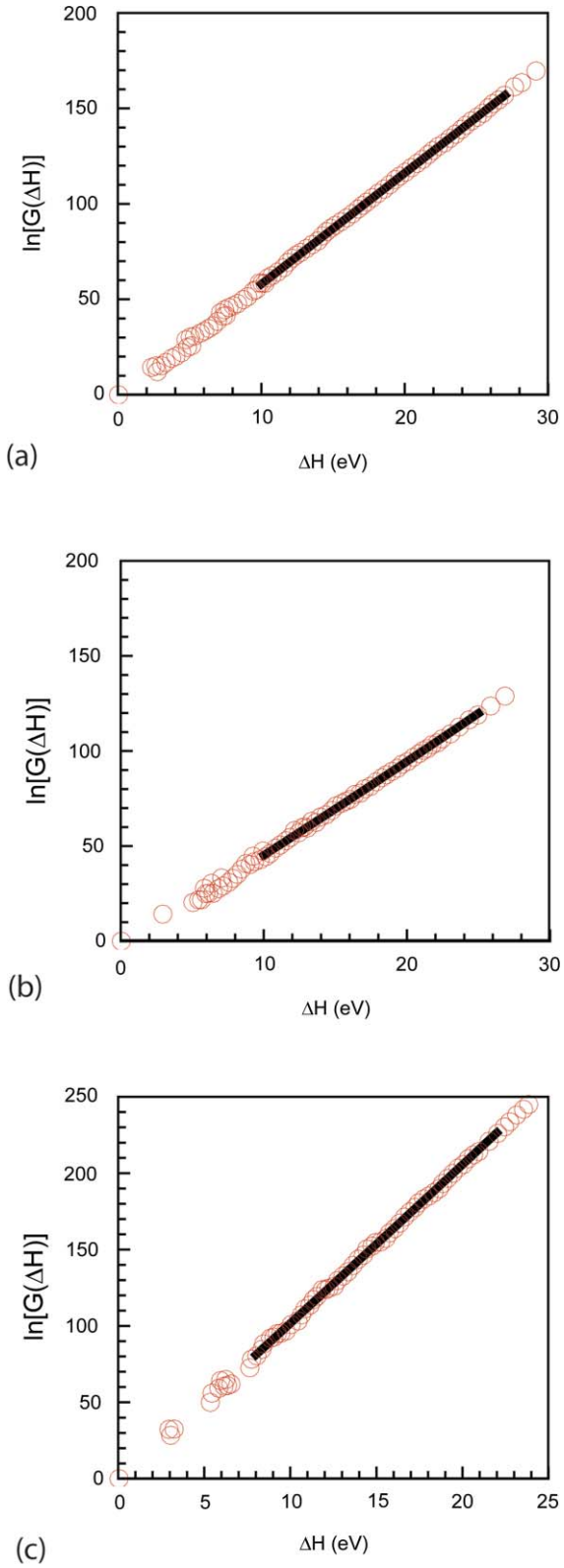

FIG. 4. Zero pressure DOS distributions for formation enthalpies for perfect crystals obtained from sampling of (a) EDIP-Si at 1900 K, SW-Si at 2225 K, and (c) EAM-Al at 1090 K. Thick black lines represent exponential fits.

Two aspects of the DOS distributions in Figure 4 are notable. First, all three DOS distributions are characterized by single exponents across the enthalpy ranges considered and therefore only a single critical temperature results. Second, all three distributions are obtained from simulations at temperatures that close to, but lower than, the homogeneous melting temperature. As such, all the sampled states in each case are macroscopically solid-like, and any highly defective, or liquid-like regions, are localized and non-percolating (see, for example inset (iv) in Figure 3). This is consistent with the observations in Ref. 18 which suggest that melting is driven by larger, critical nuclei comprised of several point defects. However, the highest enthalpy states sampled in these simulations are fairly close to melted configurations and no significant deviation from the observed exponential behavior is expected until the melting transition is reached at some higher enthalpy.

Bearing these observations in mind, it is quite straightforward to argue empirically that the effective temperature extracted from an exponentially growing DOS corresponds to the homogeneous melting temperature. Within an NPT simulation, the visit probability for a given enthalpy window is governed by both the DOS and the factor $\exp(-\beta\Delta H)$ as shown in Eq. (11). For an exponentially growing DOS, the probability distribution is therefore given by

$$P(\Delta H, \beta) = \alpha_{eff} \exp(\beta_{eff}\Delta H)\exp(-\beta\Delta H) = \alpha_{eff} \exp((\beta_{eff} - \beta)\Delta H). \quad (15)$$

As shown in Eq. (15), simulations for which $\beta > \beta_{eff}$ correspond to a bounded PDF with exponentially decreasing probabilities for visiting higher energy states. This is the case shown in Figures 1–3, in which excursions to liquid states are not observed; even the high formation enthalpy configurations shown for each model material are clearly crystalline with only localized defective regions. When $\beta < \beta_{eff}$, however, the PDF becomes divergent and higher energy states are increasingly more likely. The single-exponent nature of the DOS curves in Figure 4 then implies that the system would most likely exist in states that correspond to a bulk liquid, although what configurations in the liquid phase that would be sampled is not discernable from the portion of the overall DOS distribution that we sample in this work. At the precise point where $\beta = \beta_{eff}$, the PDF distribution is flat and all solid states become equally likely, which corresponds to the point at which the system can first access configurations up to and including some liquid states. These three situations are shown in Figure 5 for EDIP-Si. The PDFs shown in Figure 5 corresponding to the latter two cases were obtained by rescaling (using Eq. (11)) the PDF for Si in Figure 1(a) to temperatures above (top curve) and at (middle curve) the homogeneous melting temperature.

The correspondence of the DOS-derived critical temperatures to the homogeneous melting temperature was tested directly with non-equilibrium NPT-MD simulations at zero pressure. The approach employed here is similar to that used in Ref. 18. Up to ten simulations were performed for each material, starting at 1900 K for EDIP-Si, 2200 K for SW-Si, and 1050K for Al. For each simulation, the temperature was held constant for 5×10^5 steps (or about 500 ps), followed by the imposition of a temperature increase of 5 K. This cycle was repeated until the system melted. Using this approach, we found homogenous melting temperatures of 1964 ± 16 K for EDIP-Si (4096 atoms), 2243 ± 5 K for SW-Si (4096 atoms) and 1098 ± 3 K for aluminum

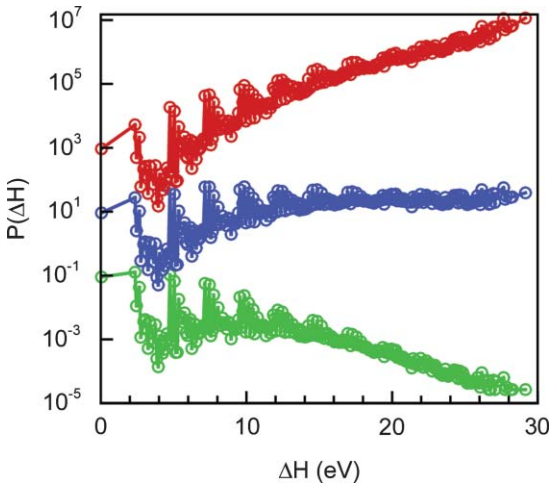

FIG. 5. Probability distribution functions for EDIP-Si at (a) $\beta > \beta_{eff}$ (lower curve), (b) $\beta \sim \beta_{eff}$ (middle curve), and (c) $\beta < \beta_{eff}$ (upper curve). The upper two curves are obtained from the lower one by rescaling the distribution in Figure 1(a) (see text).

(4000 atoms). The DOS estimates are all within 2%–5% of the non-equilibrium MD values further demonstrating that the exponent approach provides an accurate estimate of the homogeneous melting temperature while simultaneously providing a detailed view of the mechanism by which the process occurs. The influence of system size on our results is discussed below in Sec. IV A.

A. Connections to melting mechanisms

Implicit in the preceding arguments is the assumption that the DOS distributions grow with a single exponent throughout the entire range of possible formation enthalpies, presumably until the liquid states are reached. There is no fundamental reason for this to be generally true, and a DOS distribution may contain more than one distinct regions of exponential growth, each with their own growth exponent. For example, in Ref. 33, the DOS distribution for a single protein chain was clearly divided into two regions. The first (lower energy) corresponded to states during which the molecule was folded, while the second (higher energy) corresponded to unfolded states. With these considerations in mind, the single exponent observed across the entire formation enthalpy range for both Si and Al implies that homogeneous melting is governed by a single mechanism that arises from degeneracy imposed by a distribution of combinations of IV pairs. Interestingly, this single exponent is established very early on in the DOS function, even at formation energies that correspond to only a few IV pairs. This observation suggests that the nature of the critical behavior that leads to eventual homogeneous melting is already well defined in an essentially perfect crystal state that is only slightly perturbed (and certainly not liquid-like in a bulk sense).

It is also worth mentioning that the growth in the degeneracy of inherent structures is not the only factor at work in setting the value of the homogeneous melting temperature; the evolution of the vibrational entropy per inherent structure may also be important. In particular, the vibrational entropy associated with each inherent structure is expected to depend on the nature of the atomic arrangement and therefore change across the enthalpy range. Evidence for this dependency was generated in Ref. 26 for both interstitial and vacancy clusters in silicon; results in Ref. 31 also support this notion. In particular, the results in Ref. 26 suggest that the vibrational entropy of a basin grows roughly proportionally to its formation energy, i.e., the number of vibrational states also increase exponentially with formation enthalpy of an inherent structure. These findings also are qualitatively consistent with the analytical defect softening model of Stillinger and Weber.[31] This is not necessarily surprising given that defect configurations with larger formation energy tend to be larger (i.e., involve more atoms) and be more disorganized. It is therefore the combined exponential growth in the configurational and vibrational states with formation enthalpy that provides the complete pathway to homogeneous melting. A quantitative analysis of exactly how large the vibrational entropy contribution to the homogeneous melting temperature could be an interesting future study.

B. Finite size effects in the prediction of the homogeneous melting temperature

Previous studies have indicated the presence of (small) finite size effects in direct simulations of homogeneous melting.[18,48] The presence of finite size effects that persist to rather large simulations cells in homogeneous melting studies is well established, but is often essentially ignored because of the relatively small magnitude of the error for reasonably sized simulation cells. Several DOS and direct MD simulations were performed for the EDIP-Si case to probe finite size effects using periodic simulation cells containing 2744 to 238 328 atoms. The homogeneous melting temperatures as a function of system size are shown for both methods in Figure 6. Over the system size interval studied here, finite size effects are observed in both approaches, although the overall magnitude of the differences is quite small on a percentage basis—less than 5% across the large size interval considered. Moreover, the DOS approach appears to be somewhat more sensitive to finite size effects for small system sizes.

The origin of finite size effects in simulations of homogeneous melting that extend to rather large system sizes is likely due to the fact that configurations corresponding to nearly critical defect clusters are not well sampled unless the system size is very large. In Ref. 18, for example, it was found that critical clusters in Al comprised several point defects. These are not observed in smaller MD simulation cells and as a result some additional superheating must be provided to melt the system.[19] The larger finite-size sensitivity of the DOS-based simulations at small simulation cell sizes probably arises from difficulty in fully sampling configurations at higher formation energies (i.e., those that are close to critical). The difficulty arises from the fact that any DOS sampling simulation that results in melting must be terminated because it is not possible to return to the solid phase at that point. The probability of making an excursion to the melted (post-critical) state becomes exponentially more likely when the simulation temperature is increased to enable sampling of nearly critical inherent structures. The use of larger systems

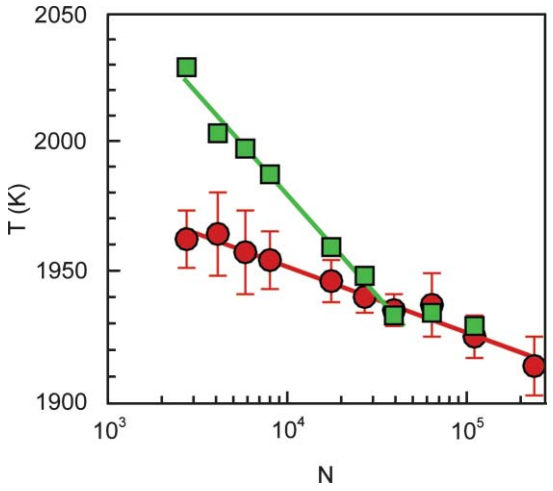

FIG. 6. Homogeneous melting temperature as a function of system size for EDIP-Si using: (a) direct MD (red circles) and (b) DOS (green squares). Lines represent power-law fits to the data (fit for DOS limited to system sizes between 2744 and 39 304).

alleviates this problem by allowing a broader distribution of IV pair clusters to exist at any one time, enhancing the sampling of these near-melting configurations.

In summary, finite size effects are intrinsically "long-ranged" in simulations of homogeneously nucleated phenomena although the effects are gradual, and in the case of melting at least, are quantitatively rather small for the system sizes considered here. By contrast, finite size effects in simulations of melting originated at a single, heterogeneous site, e.g., a nanovoid, become non-existent for systems larger than about 10 000–20 000 atoms.[49] In the heterogeneous case, the only requirement for eliminating finite size effects is that the nucleating entity be small enough relative to the simulation cell to remove direct self-interaction; this is a well-established criterion in simulations of defect formation thermodynamics.[50,51]

V. HOMOGENEOUS MELTING UNDER HYDROSTATIC COMPRESSION

There exists relatively little work regarding the simulation of homogeneous melting under applied stress. It is well understood that applied stress can strongly influence the thermodynamic melting temperature of a material, but how this effect can be interpreted in the context of the various mechanical and thermodynamic models discussed in the Introduction is not always clear. In this section we show that the DOS approach naturally incorporates the effect of applied stress into the analysis of homogeneous melting without any adjustment of the theoretical framework presented in Sec. II.

Formation enthalpy DOS distribution calculations were carried out using NPT-ensemble MD sampling runs with various applied hydrostatic pressures up to 8 GPa for both EDIP-Si (4096 atoms) and EAM-Al (4000 atoms). Some validation runs were also performed using the SW-Si model (4096 atoms) with pressures up to 5 GPa. The temperatures chosen for the sampling runs were 1750–1900 K for EDIP-Si, 1075–1450 K for EAM-Al, and 2100–2225 K for SW-Si. Different temperatures were necessary for simulations at different pressures because of the shift in homogeneous melting temperature. The resulting formation enthalpy DOS distributions are shown in Figure 7. It is immediately obvious that applied compressive pressure has opposite effects on the two materials. In the case of Si (for both potentials), the slope of the

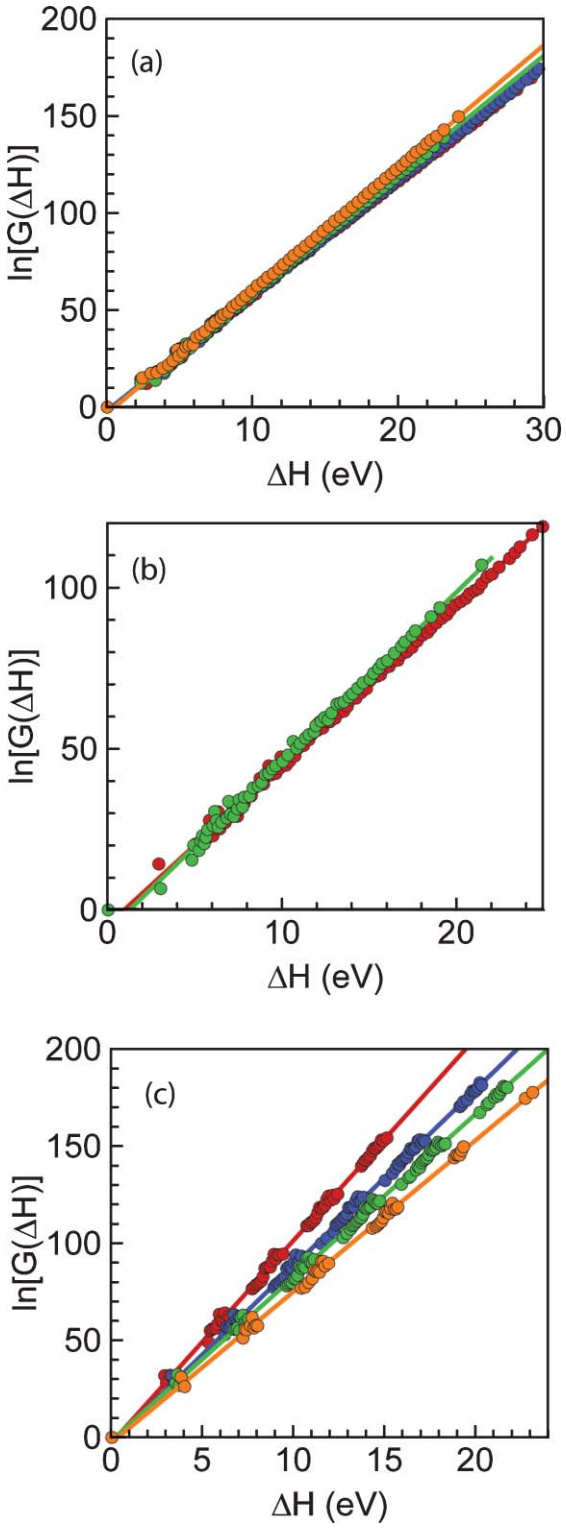

FIG. 7. Formation enthalpy DOS as a function of compressive hydrostatic pressure. (a) EDIP-Si, (b) SW-Si, and (c) Al. For all cases: red-–zero pressure, blue-–3 GPa, green-–5 GPa, and orange-–8 GPa (not all pressures shown for all systems). Sequence runs from right to left for Si cases and left to right for Al.

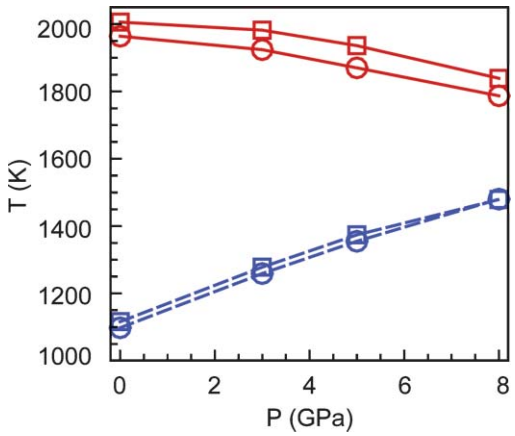

FIG. 8. Homogeneous melting temperature as a function of applied hydrostatic compression for EDIP-Si (red solid lines) and Al (blue dashed lines). Circles—direct MD results; squares—DOS.

DOS increases with pressure, while for Al it decreases; these shifts correspond to decreases and increases, respectively, in the predicted homogeneous melting temperature. The magnitude of the shift is substantially larger for Al, i.e., the homogeneous melting temperature for Al is more pressure-sensitive.

The melting temperatures extracted from the DOS curves in Figure 7 are plotted for EDIP-Si and EAM-Al as a function of compressive pressure in Figure 8. Also shown are the homogeneous melting temperatures obtained from direct MD simulations according to the method described in Sec. IV. Although there exists a systematic over-prediction of a few percent by the DOS results due to finite size effects (as discussed in Sec. IV A), the overall agreement between the direct MD and DOS predictions for both materials is excellent. The trends also qualitatively mirror the behavior that is observed in the case of thermodynamic (heterogeneously nucleated) melting, i.e., pressure increases the melting temperature for the fcc Al lattice, while Si in the diamond lattice configuration exhibits the more unusual behavior of melting point depression as pressure is increased.[52] Note that the T-P lines shown in Figure 8 are not thermodynamic coexistence boundaries but rather describe an escape from a metastable state.

Closer inspection of the Al DOS distributions in Figure 7(c) suggests a mechanism for the coupling of the homogeneous melting temperature and applied compressive pressure. The distribution of inherent structure on the formation enthalpy axis is seen to shift systematically to the right as the applied hydrostatic pressure is increased, while remaining anchored at the origin. A similar observation can be made for the EDIP-Si and SW-Si cases, although the trend is reversed and the effect is substantially smaller. The origin of this behavior is revealed by considering the formation volumes of each of the configurations represented in the DOS distributions, where the formation volume for configuration α is defined as $\Delta V_\alpha \equiv V_\alpha - V^P$. The formation volume, as defined by Aziz,[53] represents the volume change, relative to the perfect crystal, associated with the formation of a defective configuration.

Shown in Figure 9 are the contributions of the formation volumes, $P\Delta V$, to the formation enthalpy plotted as a function of the formation energy, $\Delta E \equiv \Delta H - P\Delta V$, for a large number of minimized configurations for the two Si cases and Al. For both materials, a relationship roughly of the form $P\Delta V = \xi(P)\Delta E$ is apparent at all pressures, so that $\Delta H \sim (1 + \xi(P))\Delta E$ where $\xi(P)$ is some pressure-dependent function. The function, $\xi(P)$, is large and positive for the Al case [Figure 9(c)] for all the applied pressure considered here. For EDIP-Si [Figure 9(a)], however, the formation volumes are found to be clustered around zero for all configurations at

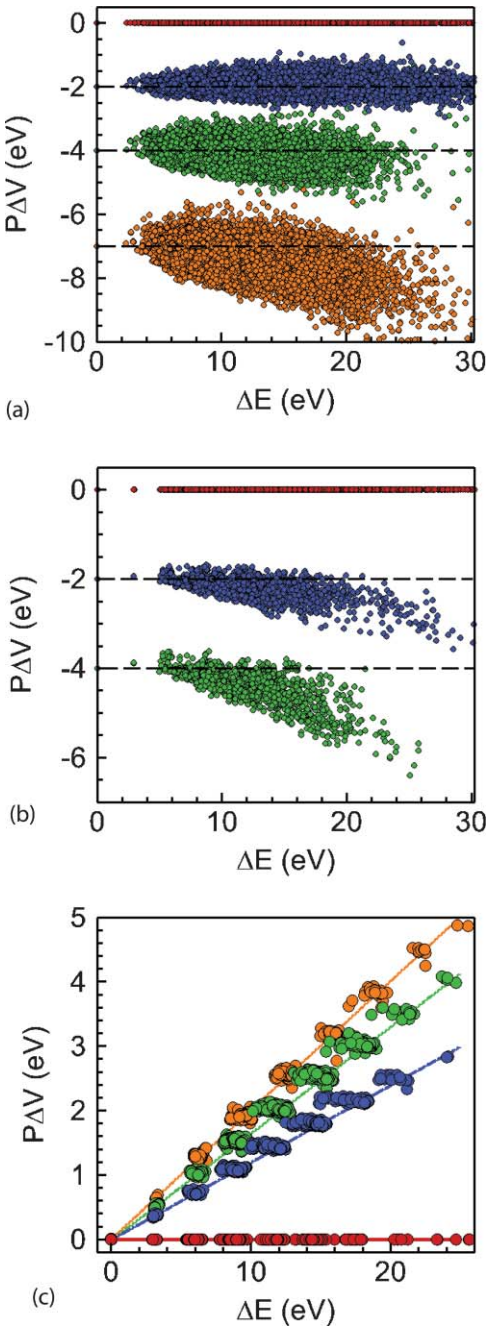

FIG. 9. Contribution of the formation volume to the formation enthalpy as a function of formation energy; (a) EDIP-Si, (b) SW-Si, and (c) Al. For all cases: red—zero pressure, blue—3 GPa, green—5 GPa, and orange—8 GPa (not all pressures shown for all systems). In (a) and (b), the formation volume contributions at 3 GPa are shifted downwards by 2 eV, at 5 GPa by 4 eV, and at 8 GPa by 7 eV for clarity. Horizontal dashed lines represent zero point energies for each of pressure case.

low pressure, removing much of the coupling between applied compression and the homogeneous melting temperature. Beyond about 5 GPa, the formation volumes begin to exhibit a highly scattered, but overall decreasing, relationship with the formation energy. At 8 GPa, most of the inherent structures exhibit negative formation volume. The trend is similar but somewhat clearer in SW-Si case (Figure 9(b)) with a stronger tendency towards negative formation volumes and less scatter; note that the 8 GPa case was omitted in the SW case. The much larger scatter in formation volumes for Si likely arises from the fact that the inherent structure landscape in Si is much rougher than that of Al due to the more open diamond lattice relative to fcc.

The results in Figure 9 suggest that the homogeneous melting temperature depends on pressure mainly through the formation volume of every defective configuration. In order for melting to proceed in the Al case, higher formation volume defective configurations must be accessed, which become increasingly unfavorable as compressive pressure increases, while the opposite is true for the Si case. This picture is supported by plotting the DOS distributions for Al and EDIP-Si at different pressures as a function of $\Delta E = \Delta H - P\Delta V$ as shown in Figure 10. In this representation, the DOS distributions become nearly independent of pressure, confirming that most of the pressure dependence of melting arises from the evolution of the formation volume with formation energy for increasingly defective configurations. Note, that some residual pressure dependence still is observed in the Al case, which suggests that the underlying energy landscape is also not completely independent of pressure, particularly once the applied compression reaches 8 GPa. The mechanism for this interaction could take place either through a modification of the vibrational entropy of individual basins or through a change of the overall roughness of the inherent structure landscape.[26]

The overall agreement between the SW and EDIP results suggests that our mechanistic conclusions are robust. While these two very dissimilar potentials predict different point defect formation properties and structures, thermodynamic melting temperatures, and thermal expansion coefficients (the EDIP one is erroneously negative at high temperature[42]), the atomistic mechanism coupling stress to homogeneous melting is unambiguously demonstrated.

We conclude this section by making a connection to thermodynamic melting. It is not unreasonable to extrapolate from the highly defective configurations accessed in the present DOS simulations to the critical liquid nuclei that actually lead to melting within the bulk crystalline phase.[16–19] The generally monotonic evolution of formation volume with formation energy across the ranges of defect configurations accessed in our simulations for both Si and Al then allows for the prediction of the sign of ΔV_M, the difference in atomic volume between the crystal and liquid states. In other words, the values of the formation volume for the highest enthalpy inherent structures that we sample in our simulations provide a reasonable lower bound on ΔV_M because these configurations correspond to nearly critical precursors to the liquid phase.

In this view it is useful to consider the Clapeyron equation which describes the pressure dependence of a phase

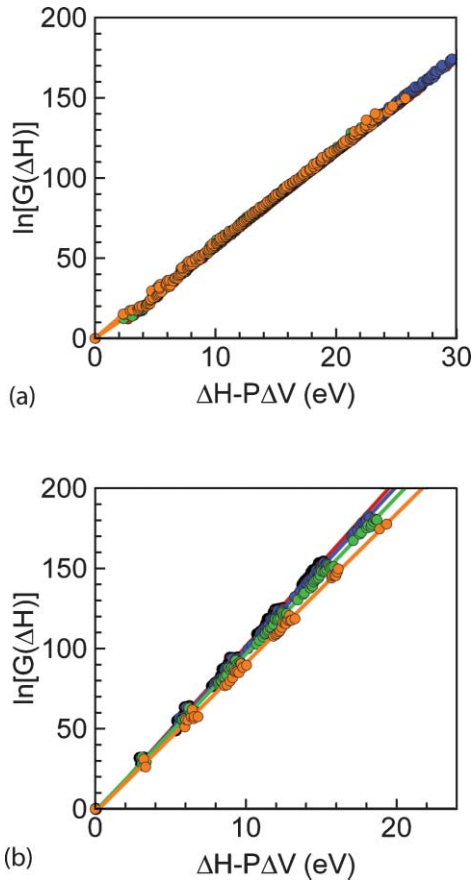

FIG. 10. DOS distributions for (a) EDIP-Si and (b) Al plotted as a function of formation energy (see text for definition) at several different applied (compressive) pressures: red—zero pressure, blue—+3 GPa, green—+5 GPa, and orange—+8 GPa.

transition

$$\left(\frac{dP}{dT}\right)_{\Delta G} = \frac{\Delta S_M}{\Delta V_M}, \tag{16}$$

where ΔS_M is entropy change upon melting, which is always positive. Eq. (16) is usually integrated along the thermodynamic coexistence line where $\Delta G = 0$, but it is also possible to invoke it along a path of constant superheating, $G_L - G_S < 0$. In view of Eq. (16), we can then state that thermodynamic melting would be subject to the same pressure dependence found in the homogeneous case. On an atomistic scale, there also appears to be a correlation between negative formation volumes for inherent structures within the crystal and a denser liquid phase, although this may or may not be universally true.

VI. CONCLUSIONS

Using equilibrium empirical potential MD simulations in the NPT ensemble, local minima (inherent structures) in the potential enthalpy landscape for two materials, Al and Si, were sampled using periodic quenches at constant applied pressure. Histograms of the visit probabilities as a function of enthalpy were then used to generate temperature-invariant density-of-states distributions for the sampled inherent structures. The resulting DOS distributions were found to grow

exponentially with formation enthalpy, exhibiting a single exponent across most of the entire enthalpy range sampled by the simulations. As expected from long-standing prior studies of homogeneous melting, the inherent structures that lead to the exponential growth in the DOS distributions for both Si and Al generally correspond to a multitude of interstitial-vacancy (or Frenkel) pair combinations.

The DOS growth exponent was demonstrated to provide a direct and accurate measure of the homogeneous melting (or maximum superheating) temperature of the perfect bulk crystal in both materials. While the relationship between a DOS growth exponent and phase transitions has been investigated in the context of other types of phase transitions, notably protein folding and order-disorder transitions in model binary alloys, its application to atomic crystal melting has not to date been widespread. Significantly, this connection can be made without the need to invoke any additional conceptual elements such as the Lindemann criterion or homogeneous nucleation theory. The fact that the exponential growth rate in the DOS distributions in both materials is described by a single exponent across the entire range of formation enthalpies suggests that homogeneous melting can be well described on the basis of the configurational and vibrational degeneracy of only a few Frenkel pairs in an otherwise perfect crystal; this notion was first proposed by the seminal work of Stillinger and Weber[31] using a simplified analytical model. The implication, therefore, is that the properties of the bulk liquid state are largely unimportant in describing homogeneous melting, and that a one-phase description is fully adequate for this special case.

The general utility of the DOS approach employed in this work is especially apparent in the latter portion of our study, where the effects of applied hydrostatic pressure on homogeneous melting were investigated. It was demonstrated that applied pressure acts primarily to alter the formation enthalpies of inherent structures that possess non-zero formation volumes. Consequently, the exponent that governs the DOS distribution is altered under the influence of hydrostatic pressure, leading to a shift in the homogeneous melting temperature. The direction of this shift was found to depend on the overall sign of the formation volumes. In the close-packed fcc-Al lattice, all formation volumes are positive, which results in increasing enthalpy under compression. In the unusual Si case, the relatively open diamond lattice leads to negative formation volumes for many (but not all) inherent structures producing a reduction in the melting temperature with applied compression. In addition to the formation volume effect, applied pressure also appears to directly alter the enthalpy landscape, either by modifying the vibrational entropy of basins or by changing the basin landscape altogether. Further studies will be required to probe these possibilities in more detail. However, for the pressures and material models considered here, less than about 15% of the melting temperature response to pressure originates from direct changes in the enthalpy landscape.

Finally we close by noting that the IS formalism employed throughout this work is readily generalizable to more complex applied stress fields and could be used with little modification to offer direct microscopic insight into phenomena such as shear-induced melting. Other types of applied fields (e.g., electric or magnetic) also are easily incorporated.

ACKNOWLEDGMENTS

This work was partially supported by NSF-NIRT award CTS-0404259. The authors are indebted to Professor Vaclav Vitek and Prof. John Crocker (University of Pennsylvania) for many useful discussions regarding this work.

[1] R. W. Cahn, Nature (London) **323**(6090), 668 (1986).
[2] J. G. Dash, Rev. Mod. Phys. **71**(5), 1737 (1999).
[3] T. E. Hsieh and R. W. Balluffi, Acta Metall. **37**(6), 1637 (1989).
[4] J. Zhong, L. H. Zhang, Z. H. Jin, M. L. Sui, and K. Lu, Acta Mater. **49**(15), 2897 (2001).
[5] Q. S. Mei, S. C. Wang, H. T. Cong, Z. H. Jin, and K. Lu, Acta Mater. **53**(4), 1059 (2005).
[6] B. J. Siwick, J. R. Dwyer, R. E. Jordan, and R. J. D. Miller, Science **302**(5649), 1382 (2003).
[7] S. Williamson, G. Mourou, and J. C. M. Li, Phys. Rev. Lett. **52**(26), 2364 (1984).
[8] A. B. Belonoshko, N. V. Skorodumova, A. Rosengren, and B. Johansson, Phys. Rev. B **73**(1), 012201 (2006).
[9] H. J. Fecht and W. L. Johnson, Nature (London) **334**(6177), 50 (1988).
[10] L. C. Gallington and A. Bongiorno, J. Chem. Phys. **132**(17), 174707 (2010).
[11] J. L. Tallon, Nature (London) **342**(6250), 658 (1989).
[12] F. A. Lindemann, Physik. Z. **11**, 609 (1910).
[13] J. J. Gilvarry, Phys. Rev. **102**(2), 308 (1956).
[14] M. J. Born, J. Chem. Phys. **7**, 591 (1939).
[15] K. Lu and Y. Li, Phys. Rev. Lett. **80**(20), 4474 (1998).
[16] S. N. Luo, L. Q. Zheng, A. Strachan, and D. C. Swift, J. Chem. Phys. **126**(3), 034505 (2007).
[17] Z. H. Jin, P. Gumbsch, K. Lu, and E. Ma, Phys. Rev. Lett. **87**(5), 055703 (2001).
[18] M. Forsblom and G. Grimvall, Nature Mater. **4**(5), 388 (2005).
[19] L. Q. Zheng, Q. An, Y. Xie, Z. H. Sun, and S. N. Luo, J. Chem. Phys. **127**(16), 164503 (2007).
[20] F. H. Stillinger and T. A. Weber, Phys. Rev. A **25**(2), 978 (1982).
[21] Goldstei. M, J. Chem. Phys. **51**(9), 3728 (1969).
[22] F. Sciortino, W. Kob, and P. Tartaglia, Phys. Rev. Lett. **83**(16), 3214 (1999).
[23] S. Buchner and A. Heuer, Phys. Rev. E **60**(6), 6507 (1999).
[24] P. G. Debenedetti and F. H. Stillinger, Nature (London) **410**(6825), 259 (2001).
[25] S. S. Kapur, M. Prasad, J. C. Crocker, and T. Sinno, Phys. Rev. B **72**(1), 014119 (2005).
[26] S. S. Kapur, A. M. Nieves, and T. Sinno, Phys. Rev. B **82**(4), 045206 (2010).
[27] T. V. Bogdan, D. J. Wales, and F. Calvo, J. Chem. Phys. **124**(4), 044102 (2006).
[28] F. Calvo and D. J. Wales, J. Chem. Phys. **131**(13), 134504 (2009).
[29] J. C. Mauro, R. J. Loucks, J. Balakrishnan, and S. Raghavan, J. Chem. Phys. **126**(19), 194103 (2007).
[30] C. Chakravarty, P. G. Debenedetti, and F. H. Stillinger, J. Chem. Phys. **126**(20), 204508 (2007).
[31] F. H. Stillinger and T. A. Weber, J. Chem. Phys. **81**(11), 5095 (1984).
[32] C. Bichara, J. P. Gaspard, and J. C. Mathieu, J. Chem. Phys. **89**(7), 4339 (1988).
[33] N. Nakagawa and M. Peyrard, Proc. Natl. Acad. Sci. U.S.A. **103**(14), 5279 (2006).
[34] N. Nakagawa and M. Peyrard, Phys. Rev. E **74**(4), 041916 (2006).
[35] Y. Mishin, M. R. Sorensen, and A. F. Voter, Philos. Mag. A **81**(11), 2591 (2001).
[36] M. Potuzak, J. C. Mauro, T. J. Kiczenski, A. J. Ellison, and D. C. Allan, J. Chem. Phys. **133**(9), 091102 (2010).
[37] M. Z. Bazant, E. Kaxiras, and J. F. Justo, Phys. Rev. B **56**(14), 8542 (1997).
[38] M. I. Mendelev, M. J. Kramer, C. A. Becker, and M. Asta, Philos. Mag. **88**(12), 1723 (2008).
[39] F. H. Stillinger and T. A. Weber, Phys. Rev. B **31**(8), 5262 (1985).

[40]T. A. Frewen, S. S. Kapur, W. Haeckl, W. von Ammon, and T. Sinno, J. Cryst. Growth **279**(3–4), 258 (2005).
[41]S. S. Kapur and T. Sinno, Phys. Rev. B **82**(4), 045205 (2010).
[42]P. Keblinski, M. Z. Bazant, R. K. Dash, and M. M. Treacy, Phys. Rev. B **66**(6), 064104 (2002).
[43]S. J. Plimpton, J. Comput. Phys. **117**, 1 (1995).
[44]C. L. Kelchner, S. J. Plimpton, and J. C. Hamilton, Phys. Rev. B **58**(17), 11085 (1998).
[45]J. G. Dai, J. M. Kanter, S. S. Kapur, W. D. Seider, and T. Sinno, Phys. Rev. B **72**(13), 134102 (2005).
[46]J. Dal, W. D. Seider, and T. Sinno, Mol. Simul. **32**(3–4), 305 (2006).
[47]W. G. Hoover, B. L. Holian, and A. C. Hindmarsh, J. Chem. Phys. **57**(5), 1980 (1972).
[48]A. B. Belonoshko, S. Davis, N. V. Skorodumova, P. H. Lundow, A. Rosengren, and B. Johansson, Phys. Rev. B **76**(6), 064121 (2007).
[49]X. M. Bai and M. Li, Nano Lett. **6**(10), 2284 (2006).
[50]T. Sinno, Z. K. Jiang, and R. A. Brown, Appl. Phys. Lett. **68**(21), 3028 (1996).
[51]M. Prasad and T. Sinno, Appl. Phys. Lett. **80**(11), 1951 (2002).
[52]D. A. Young, *Phase Diagrams of the Elements* (University of California Press, Berkley, CA, 1991).
[53]M. J. Aziz, Appl. Phys. Lett. **70**(21), 2810 (1997).